VOF for the Free Surface Flows of Breaking Waves

Chih-Min Hsieh[1] Tai-Wen Hsu[2] Chin-Yen Tsai[2] Zbigniew Pruszak[3]

ABSTRACT

A numerical model for simulating breaking waves on a sloping bed was developed. A RANS (Reynolds Averaged Navier-Stokes) based model and the embedding method for bluff body flows on a solid object were employed by taking account of the fully nonlinear, viscous and turbulent effects on the wave breaking problem. Based on a staggered computational mesh, an explicit numerical algorithm is employed with a predictor-corrector procedure of pressure and velocity field computation. To track the free surface movement with wave breaking, the volume of fluid (VOF) method is implemented. Coupling the VOF and the embedding method, the treatment on free surface problem and complex bottom topography can be easily accomplished. Comparing with the existing experiments, a good agreement is found between numerical results and measured data.

1. INTRODUCTION

When waves reach a beach and enter water that is nearly as deep as the waves are high, they become unstable and break with the crest thrown forward as the wave disintegrates into bubbles. Wave breaking is one of the most commonly observed features of water waves propagating from deep water to shallow water, over a sloping bottom. On the other hand, submerged coastal structures are also frequently used for coastal protection from wave attack. The main purpose of this structure is to reduce the transmitted wave energy by reflecting waves and dissipating wave energy over the structure by breaking up the propagating waves.

When wave breaking occurs, a large amount of wave momentum will be released to the surface layer of surf zone. Breaking waves also play an essential role in the surf zone for an entire coastal process. For example, strong turbulence produced by breaking waves could stir up sediment particles into the flow. Changes of sediment subsequently result in sediment transport may cause beach erosion and related coastal disasters such as wave overtopping, coastal flooding and failure of coastal structures, and so on.

Notably the existing potential theories describing the evolution of wave profile of breaking waves normally neglect the effect of viscosity and turbulence. In order to simulate the process of real flow interaction which takes place on sea bottom or around submerged structures, the full Navier-Stokes equations with exact free surface boundary conditions should be solved. Computational efficiency and reliability are key elements of the model for simulating wave breaking process. In this research, we developed a numerical model to calculate the flow dynamics and water free surface deformation for periodic waves traveling on different types of sloping bottom with breaking and energy dissipation. The feasibility of the numerical model was verified through a series of comparisons of numerical results with the existing analytical solutions and the

1 National Kaohsiung Marine University, Kaohsiung, Taiwan,R.O.C.
2 National Cheng Kung University, Tainan, Taiwan, R.O.C.
3 Institute of Hydro-Enginering, Polish Academy of Sciences, Gdańsk, Poland
Email address: llmmbb12@so-net.net.tw (Chin-Yen Tsai)

experimental data. The good agreements demonstrate the satisfactory performance of the developed numerical model.

The purpose of this paper is to perform numerical simulations of numerical simulations in investigating the deformation of periodic waves and breaking process on a sloping bed by the VOF method and embedding method. The applicability of the VOF method on the wave breaking problem is discussed. The mean flow pattern and turbulent kinetic energy distribution under wave breaking are explored using the developed numerical model.

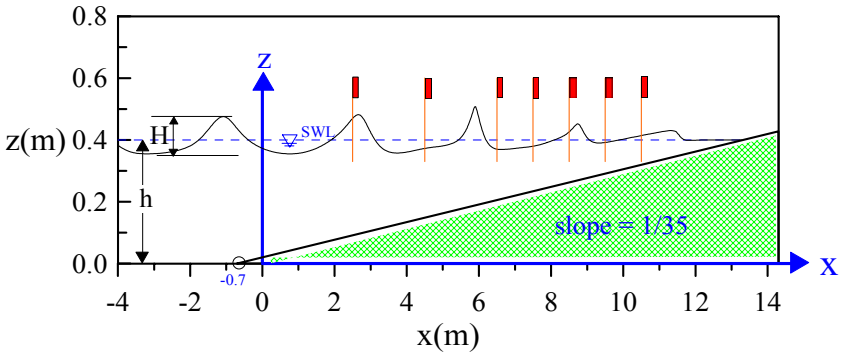

Fig1. Schematic diagram of periodic wave train over a sloping bed

2. GOVERNING EQUATIONS

The physical problem considered in this study is the propagation of a two-dimensional periodic wave train traveling toward the sloping bed and the varying topography. The Cartesian coordinate system is employed in this study as shown in Fig. 1. Herein, h denotes the quiescent water depth in front of the sloping beach, H the wave height of incident periodic waves.

The Reynolds decomposition method is applied to simulate the turbulence effect. The governing equations which describe the mean quantities of the flow field for unsteady incompressible turbulent flows are denoted as

continuity equation

$$\frac{\partial U}{\partial x}+\frac{\partial W}{\partial z}=0 \tag{1}$$

and momentum equations

$$\frac{\partial U}{\partial t}+U\frac{\partial U}{\partial x}+W\frac{\partial U}{\partial z}=-\frac{\partial P}{\partial x}+(\nu_t+\nu)\nabla^2 U+\frac{\partial}{\partial x}(\nu_t\frac{\partial U}{\partial x})+\frac{\partial}{\partial z}(\nu_t\frac{\partial W}{\partial x})-\frac{2}{3}\frac{\partial k}{\partial x} \tag{2}$$

$$\frac{\partial W}{\partial t}+U\frac{\partial W}{\partial x}+W\frac{\partial W}{\partial z}=-\frac{\partial P}{\partial z}+(\nu_t+\nu)\nabla^2 W+\frac{\partial}{\partial x}(\nu_t\frac{\partial U}{\partial z})+\frac{\partial}{\partial z}(\nu_t\frac{\partial W}{\partial z})-\frac{2}{3}\frac{\partial k}{\partial z}-g \tag{3}$$

in which x and z are the coordinates in a fixed Cartesian system respectively, t is the time, U and W are the mean velocity components in the x- and z-directions, respectively, P is pressure, g is the gravitational acceleration, ν_t is the eddy viscosity, ν is the molecular viscosity, $\nabla=(\partial/\partial x,\partial/\partial z)$ is the gradient operator; and k is the turbulent kinetic energy.

The standard $k-\varepsilon$ model is employed here to resolve the eddy viscosity in the present study. The eddy viscosity is determined by the turbulent kinetic energy *k* and energy dissipation rate ε using the following formula

$$\nu_t = \frac{C_\mu k^2}{\varepsilon} \tag{4}$$

The governing equations (1)-(3) are closed by the transport equations of the Turbulent Kinetic Equation (TKE) and Energy Dissipation Equation (EDE):

$$\frac{\partial k}{\partial t} + U\frac{\partial k}{\partial x} + W\frac{\partial k}{\partial z} = \nabla\cdot\left[(\nu + \frac{\nu_t}{\sigma_k})\nabla k\right] + Prod - \varepsilon \tag{5}$$

$$\frac{\partial \varepsilon}{\partial t} + U\frac{\partial \varepsilon}{\partial x} + W\frac{\partial \varepsilon}{\partial z} = \nabla\cdot\left[(\nu + \frac{\nu_t}{\sigma_\varepsilon})\nabla \varepsilon\right] + C_1\nu_t\frac{\varepsilon}{k}Prod - C_2\frac{\varepsilon^2}{k} \tag{6}$$

where Prod term represents the production of turbulent kinetic energy denoted as

$$Prod = \nu_t\left[2(\frac{\partial U}{\partial x})^2 + 2(\frac{\partial W}{\partial z})^2 + (\frac{\partial U}{\partial z} + \frac{\partial W}{\partial x})^2\right] \tag{7}$$

Herein, σ_k, σ_ε, C_μ, C_1 and C_2 are empirical coefficients and are taken to be $\sigma_k = 1.0$, $\sigma_\varepsilon = 1.3$, $C_\mu = 0.09$, $C_1 = 1.44$ and $C_2 = 1.92$ as suggested by Rodi (1980) and Hsu et al. (2004).

3. INITIAL AND BOUNDARY CONDITIONS

For the above-mentioned initial boundary value problem, appropriate initial condition and boundary conditions are required. At the beginning of the flow simulation, the initial flow field is assumed to be still, so that the velocity components *U* and *W* are both set to be zero throughout the whole flow field. The hydrostatic pressure is utilized for the first stage of the pressure field. For the turbulence quantities *k* and ε, the specification of initial condition requires more careful treatments to avoid singular terms existing in the EDE when *k* = 0. Following Lin and Liu (1998), we specify the initial value by setting $k = U_p^2/2$, where $U_p = A_1 C_p$, U_p and C_p are the horizontal mean velocity and wave celerity on the upstream boundary, respectively. A_1 is taken to be 2.5×10^{-3} in the present computation.

There are four boundary conditions considered in this flow, including the upstream, downstream, free surface, and solid surface boundaries. In the numerical computations the free-surface displacements and the velocity components of two kinds of periodic waves are given as the inflow conditions at *x* = 0, the upstream end of domain. The first kind of periodic wave is co-sinusoidal wave based on linear wave theory. The other incident wave is Cnoidal (Cn) wave. The wave profile can be expressed as (Ispbe et al., 1978)

$$h_s = h + \eta = h\sum_{n=0}^{3} A_n \,\mathrm{cn}^{2n}\left[2\kappa(\frac{x}{L} - \frac{t}{T})\right] \tag{8}$$

where $\kappa = 2\pi/L$, *L* is the wave length, and

$$U = \sqrt{gh}\sum_{n=0}^{3}\sum_{m=0}^{2} B_{nm}\left(\frac{h+z}{h}\right)^{2m} \mathrm{cn}^{2n}\left[2k\left(\frac{x}{L}-\frac{t}{T}\right)\right] \tag{9}$$

$$W = \sqrt{gh}\cdot \mathrm{sn}\left[2\kappa\left(\frac{x}{L}-\frac{t}{T}\right)\right]\cdot \mathrm{dn}\left[2\kappa\left(\frac{x}{L}-\frac{t}{T}\right)\right]\times \frac{4\kappa h}{L}\sum_{n=1}^{3}\sum_{m=1}^{2}\frac{n}{2m+1}B_{nm}\left(\frac{h+z}{h}\right)^{2m+1}\cdot \mathrm{cn}\left[2\kappa\left(\frac{x}{L}-\frac{t}{T}\right)\right] \tag{10}$$

Coefficients A_n and B_{nm} in Eqs. (8) to (10) are determined according to Isobe et al.'s theory. cn, sn, and dn are Jacobian elliptic function. On the other hand, a radiation boundary condition proposed by Orlanski (1976) is imposed at the downstream to let progressive waves outgoing without reflection.

The boundary conditions on the solid surfaces including the bed and the undulation surfaces are assumed to be impermeable and non-slip. That is, the velocity components *U* and *W* are equal to zero at those boundaries. On the free surface boundary, one kinetic and two dynamic boundary conditions are used. They are denoted as,

$$\frac{\partial h_s}{\partial t}+U\frac{\partial h_s}{\partial x}=W \text{ , at } z= h_s(x,t) \text{ ,} \tag{11}$$

$$2\frac{\partial h_s}{\partial x}\left(\frac{\partial U}{\partial x}-\frac{\partial W}{\partial z}\right)+\left[\left(\frac{\partial h_s}{\partial x}\right)^2-1\right]\left(\frac{\partial U}{\partial z}+\frac{\partial W}{\partial x}\right)=0 \text{ , at } z=h_s(x,t) \text{ ,} \tag{12}$$

$$P/\rho=\frac{2(\nu+\nu_t)}{1+\left(\frac{\partial h_s}{\partial x}\right)^2}\left[\left(\frac{\partial h_s}{\partial x}\right)^2\frac{\partial U}{\partial x}-\frac{\partial h_s}{\partial x}\left(\frac{\partial U}{\partial z}+\frac{\partial W}{\partial x}\right)\frac{\partial W}{\partial z}\right], \text{ at } z=h_s(x,t) \text{ ,} \tag{13}$$

Boundary conditions for *k* and ε on a free surface are (Launder, 1989) are

$$\frac{\partial k}{\partial n}=0 \text{ , } \frac{\partial \varepsilon}{\partial n}=0 \text{ ,} \tag{14}$$

where *n* is the normal direction of a free surface.

3.1 Volume of Fluid Method

Like other studies of free surface flows, we also encounter difficulties in treating the free surface boundary conditions. Thus an suitable way of finding the free surface is important in numerical calculation. The piecewise linear interface calculation (PLIC) method developed based on the concept of VOF is adopted in this study to track the complicatedly and rapidly changed water surfaces during wave breaking.

The main principle of VOF is established according to the material transport conservation theory (Hirt and Nichols, 1981). Based on this theory, we can define a variable called the VOF function, F(x,z,t) which represents the fractional volume of fluid occupied on every cell and the mechanism can be described by the following formula

$$\frac{\partial F}{\partial t}+U\frac{\partial F}{\partial x}+W\frac{\partial F}{\partial z}=0 \tag{15}$$

The variable *F* ranging from 0 to 1 is also defined at the center of a computational cell. That is, the computational cells can be divided into three kinds. A cell full of fluid is called a fluid cell and has the value of 1. On the other hand, if a cell does not contain

any fluid, it will be called an empty cell and has zero value. Lastly, cells that are partially filled with fluid are called surface cells and have the values between 0 and 1.

To solve Eq. (15) and reconstruct the free surface, Gueyffier et al. (1999) proposed a VOF/PLIC algorithm with second order accuracy. The procedure for this algorithm is divided into two steps: a reconstruction step and a propagation step. The first step is the determination of the orientation of the segment and the area occupied by water in a surface cell with the known volume fraction *F*. After reconstructing the free surface, its motion by the underlying flow field need to be modeled appropriately in the propagation step. In the present study, a Lagragian advection technique is utilized to advect the interface segments and evaluate the corresponding volume fluxes in the fluid cell.

3.2 Embedding Method

The embedding method proposed by Ravoux et al. (2003). The embedding method refers to a scheme for flows in the vicinity of stationary or moving solid bodies using a space-filling Cartesian grid that passes through the solid bodies as well. The governing equations for fluid flow are solved everywhere, including the cells which are occupied by the solid body. The presence of the solid body is accounted for, however, by adding a force field to the momentum equations in those cells that are fully or partially occupied by the solid phase. The magnitude and direction of this body force density is determined at each time step by requiring the value of the velocity in those cells to match the prescribed velocity of the solid body. This is done with the aid of a volume-fraction field that determines what fraction of each computational cell in the Cartesian grid is occupied by the solid phase. In cells where the solid volume fraction is unity, the velocity is set exactly equal to that of the body, and in those where the volume fraction is between zero and one, the velocity is only adjusted partially, in proportion to the volume fraction. Cells which are free from the solid and have a volume fraction of zero do not possess this body-force and are not affected in that step of the computation.

4. MODEL VALIDATION

The physical problem considered here is the propagation of a two-dimensional periodic wave train shoaling on a sloping bottom. Three cases of different bottom types including uniform slope, bar type and step type are chosen to validate the developed model. Table 1 shows the numerical conditions for each test case.

Fig. 1 shows the schematic view of the numerical wave channel for case A where the distance between x = 0 m and the begin of the slopping bed is 0.7 m and z = 0 m is

Table1. Numerical conditions of test cases for model validation

Case	Bottom type	Wave height H (m)	Wave period T (s)	Wave profile
A	uniform slope	0.125	2.0	Cn wave
B	bar type	0.07	0.94	co-sinusoidal wave
C	step type	0.07	1.18	co-sinusoidal wave

located at the bottom. Ting and Kirby (1994) performed experiments to investigate the evolution of a spilling breaking Cn wave over the 1/35 slope. The incident wave heights H_i and period T in the constant water depth are 0.125 m and 2.0 s for the spilling

breaker, respectively. They measured time histories of surface elevation at 4 various locations over the bed. In the numerical simulation, the computational domain is 20 m long and 0.8 m high. Fig. 2 is the comparison of the water elevations at the shoaling regions and a bore region. It reveals very close agreements existed between the predicated elevations shown in solid line and the measurements denoted as circles.

Fig. 3 shows the comparison of the predicated wave crest, trough and mean water level distribution, among Ting and Kirby's data, and numerical results given by Bradford (2000) and present model. The predicated wave crest profile agrees with other's results except for the values in the region x = 5~7 m. The wave breaking happens at x = 6.4 m, so it is a critical region to compare. Furthermore, the predicated wave trough profile agrees with their data well. The mean water level profile is very interesting, because it is lower then the still water level before the wave breaking point x = 6.4 m and arises gradually after the breaking point.

The comparison of the averaged velocity components are presented in Fig. 4. The overall agreements between computed and measured results are found to be good at different locations in the surf zone. From Figs. 2 and 4, it is demonstrated that the developed model is capable to simulate the wave transformation and flow field for spilling breaking wave on a uniform slope bottom.

At the post-breaking stage, the wave energy may recovery following another occurrence of wave breaking if the local water depth does not decrease gradually shoreward. Therefore, numerical simulations of periodic waves propagating on composite slope bottom are carried out to evaluate the performance of the present model on wave recovery. Nagayama (1983) measured the wave deformations on a bar type and step type bottom as shown in the lower row of Fig. 5. The wave conditions for these two laboratory experiments are listed in Table 1 as cases B and C, respectively.

Fig. 5 shows the computed wave heights in upper row, the surface elevations at different time steps and the envelopes in the middle row, and the profiles of composite slope bottoms in the lower row. It is seen clearly that the recovery of wave energy take places while the post-breaking wave propagating on the section with increasing or constant water depth. Moreover, the locations of first and second breaking points are well predicted in comparing with the experimental data. In general, the present model results agree well with the measurements but slightly overestimated in the surf zone for case C.

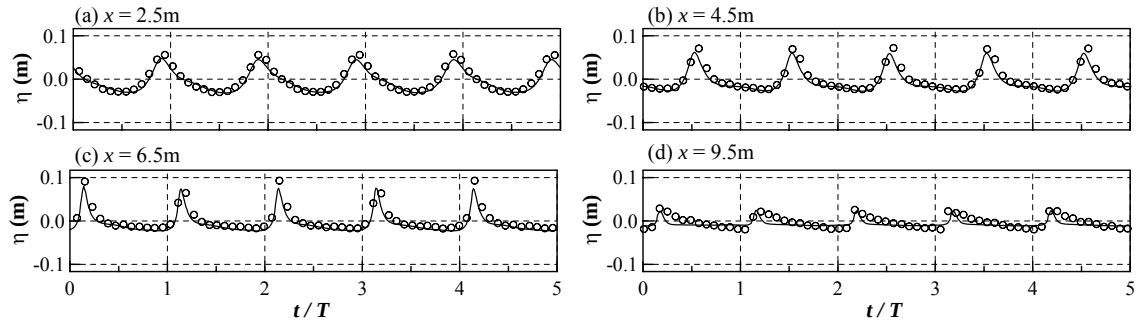

Fig2. Comparisons of simulated (solid line) and measured (circles, Ting and Kirby 1994) water elevations at the shoaling region (a)-(c) and the bore region (d)

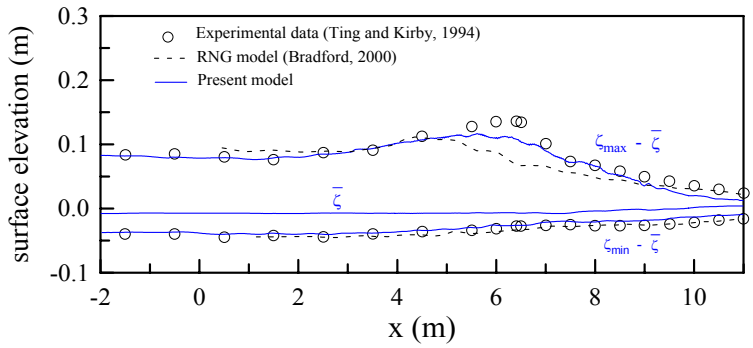

Fig3. Computed and measured spatial distribution wave crest, mean water level, and wave trough

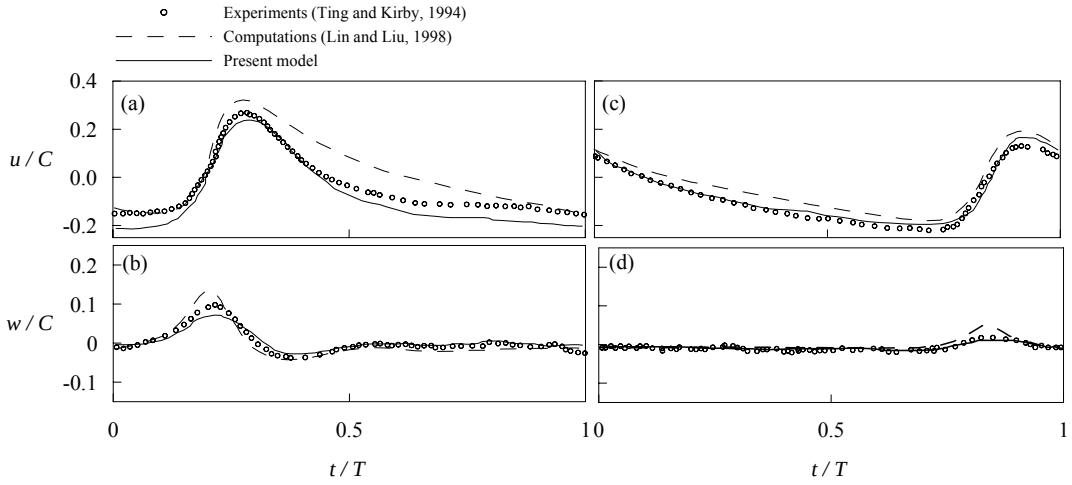

Fig4. Comparisons of averaged horizontal (a, c) and vertical velocities (b, d) at different locations in the surf zone

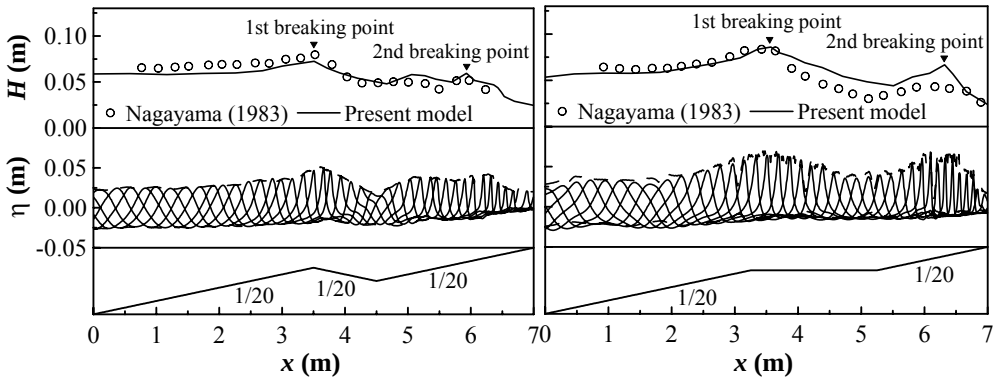

Fig5. Computed wave heights and wave envelopes for two cases of different composite slope bottoms

5. RESULTS AND DISCUSSION

In this section, we present some discussion on mean flow field and turbulent kinetic transport mechanism under wave breaking on sloping bottom using our numerical results. Contours of turbulent kinetic energy k are shown in Fig. 6 at different phases. The initial phases is set as the wave crest passes the breaking point, i.e. x = 6.4 m. It is found that the k is formed behind the wave crest. When it travels, the wave becomes steeper and k increases gradually. We also found that there is substantial turbulent kinetic energy generated at the solid boundary associated with the wave crest. Under the spilling breaking wave, the turbulent kinetic energy continues to dissipate in the bore region. This is due to the high shear rates at the wavefront which generates significant levels of k at the lower front face of the wave. After that, the production of k continues as the wave transforms into a bore and overtakes the decaying turbulence from the previous breaking wave.

Figs. 7 and 8 present the sequence of variation of the simulated streamlines and vorticity fields for case B of bar type bottom in a wave period. The vorticity is calculated by the following equation $\Omega = \partial U / \partial z - \partial W / \partial x$. In Fig. 7, the wave profile at the recovery stage is quite different from that expected for a spilling breaker. The wave crest of recovery wave is much flatter with a relatively mild leading wavefront. Fig. 8 shows that the vorticity generated by waves is initiated at the wavefront just before the breaking point for both the first and second breaking scenarios. It is noted that the computed vorticity in the second breaking is larger that in the first breaking.

6. CONCLUDING REMARKS

A two-dimensional free-surface flow model used in this study is established bydirectly solving Reynolds averaged Navier-Stokes (RANS) equations and the continuity equation. The VOF/PLIC and embedding method are adopted to track the free surface and to treat the complex solid boundary on a Cartesian grid, respectively. An explicit numerical algorithm is employed with a predictor-corrector procedure of pressure and velocity field. By applying the developed model to the problems of periodic waves breaking on different types of sloping bottom, we found that the model results compare well with the experimental data. Additionally, it is demonstrated to provide reliable information concerning wave breaking and wave recovery on a composite slope bottom.

Detailed analysis of numerical results also shows that the turbulent kinetic energy and vorticity are primarily located above the wave trough. The turbulent kinetic energy is convected and diffused to the back face of the wave, and continues to dissipate while the breaking wave moves towards the shore. As the second wave breaking takes place after the recovery of wave energy, noted that the vorticity in the bore region is larger than those in other regions.

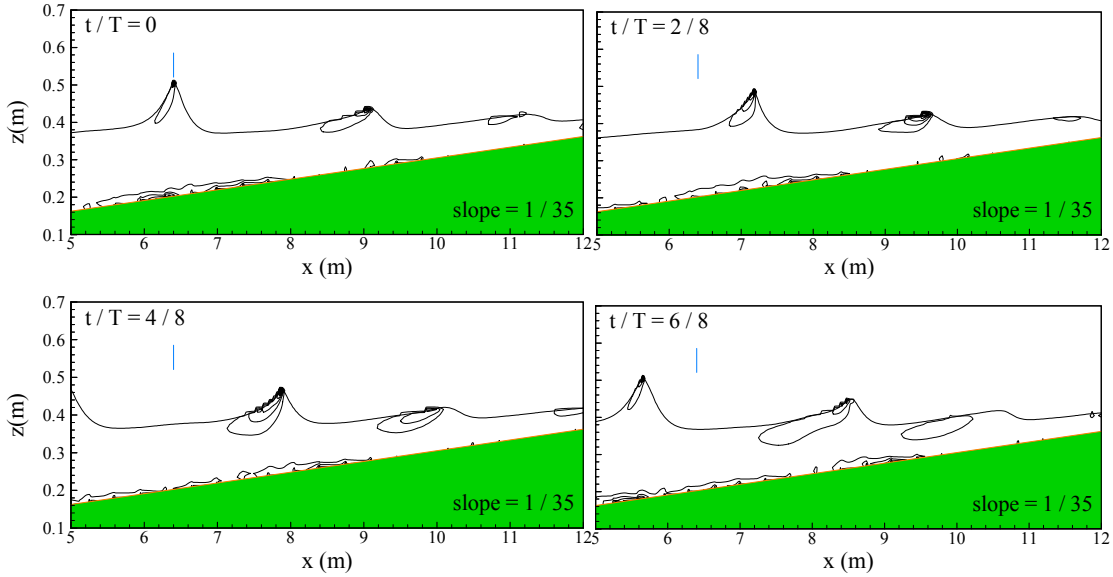

Fig6. Sequence of variation of the simulated turbulent kinetic energy for case A in a wave period

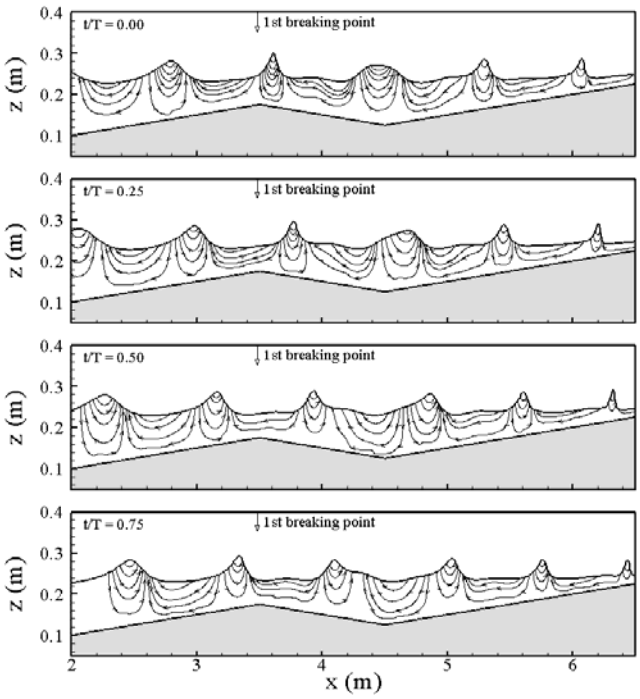

Fig7. Sequence of variation of the simulated streamlines for case B in a wave period

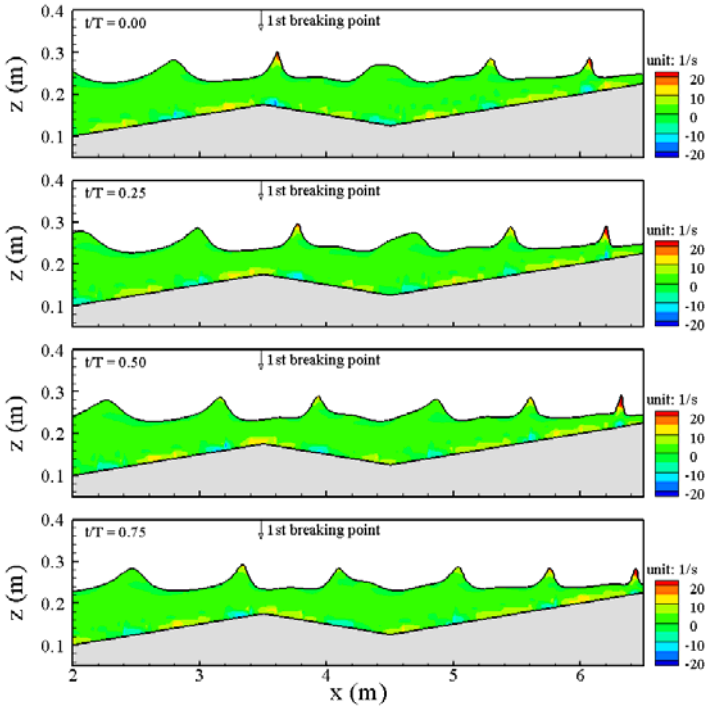

Fig8. Sequence of variation of the simulated vorticity fields for case B in a wave period

ACKNOWLEDGMENTS

This research was supported by the Landmark Project of National Cheng-Kung University, Taiwan.

REFERENCES

[1] Bradford, S.F., 2000. Numerical Simulation of Surf Zone dynamics, J. Waterw., Port, Coast. Ocean Eng. 126, pp. 1-13.

[2] Gueyffier, D., Li, J., Nadim, A., Scardovelli, R. and Zaleski, S., 1999. Volume-of-Fluid Interface Tracking with Smoothed Surface Stress Methods for Three-dimensional Flows. J. Comput. Phys. 152, pp. 423-456.

[3] Hirt, C.W. and Nichols, B.D., 1981. Volume of Fluid (VOF) Method for Dynamics of Free Boundaries. J. Comput. Phys. 39, pp. 201-225.

[4] Hsu, T.W., Hsieh , C.M. and Hwang, R.R., 2004. Using RANS to Simulate Vrtex Generation and Dissipation around Impermeable Submerged Double Breakwaters. Coast. Eng. 51, pp. 557-579.

[5] Isobe, M., Nishimura, H. and Horikawa, K., 1987. Expression of Permanent Type. Bull. Fac. Eng. Yokohama Nat. Univ. 31, pp. 29-57.

[6] Launder, B.E., 1989. Second-moment Closure and Its Use in Modeling Turbulent Industrial Flows. Int. J. Numer. Methods Fluids 9, pp. 963-985.

[7] Lin, P., and Liu, P.L.F., 1998. A Numerical Study of Breaking Waves in the Surf Zone. J. Fluid Mech. 359, pp. 239-264.

[8] Orlanski, I., 1976. A Simple Boundary Condition for Unbounded

Hyperbolic Flows. J. Comput. Phys. 21, pp. 251-269.
[9] Ravoux J.F., Nadim, A. and Haj-Hariri, H., 2003. An Embedding Method for Bluff Body Flows: Interaction of Two Side-by-side Cylinder Wakes, Theoret. Comput. Fluid Dynamics 16, pp. 433-466.
[10] Rodi, W. 1980. Turbulent Models and Their Applications in Hydraulics-A State of the Art Review. International Association for Hydraulics Research, Delft.
[11] Ting, F.C.K., and Kirby, J.T., 1994. Observation of Undertow and Turbulence in a Laboratory Surf Zone, Coast. Eng. 24, pp. 51-80.
[12] Nagayama, S. 1983. Study on the Change of Wave Height and Energy in the Surf Zone. Bachelor Thesis, Yokohama National Unversity, Japan, pp. 80.